On the Deployment Problem in Cell-Free UAV Networks

Carles Diaz-Vilor,[1] Angel Lozano,[2] and Hamid Jafarkhani[1]

***Abstract*—Cell-free (CF) structures are expected to be a game changer for beyond-5G wireless networks. With every user potentially communicating with every base station, cooperation at a central processing point is poised to provide much higher spectral efficiencies. At the same time, the growing interest in unmanned aerial vehicles (UAVs) makes CF-UAV networks an appealing scenario. This paper investigates the uplink of a CF network where UAVs serve as flying base stations. The optimization of the UAV locations is shown to markedly increase the minimum local-average signal-to-interference-plus-noise ratio, which in turn increases the spectral efficiency. The improvements are associated to pilot contamination and to geometry.**

***Index Terms*—Cell-Free, UAV, deployment optimization**

I. Introduction

The evolution towards software-defined architectures motivates the interest in centralized, possibly cloud-based, radio access networks [1]. The corresponding base stations consist only of antennas and RF stages, with the baseband processing concentrated at some suitable point. This naturally invites a cell-free (CF) structure where every user potentially connects to every base station, and takes the principles of cell cooperation to the limit [2]–[8]. To render CF networks scalable while retaining their main features, the users connecting to each base station can be limited to appropriate subsets [7].

There is growing interest in unmanned aerial vehicles (UAVs) serving as flying base stations (FBSs), but most of the related work has taken place within the confines of the cellular paradigm [9]–[16]. The challenge of deploying FBSs for an optimal performance, in particular, has received considerable attention [17]–[19]. However, the problem of deploying FBSs in CF-UAV networks remains largely unexplored. For the sake of tractability, existing works on FBS deployment and trajectory optimization broadly assume simplified channel models and perfect channel-state information (CSI) [11]–[13].

The present paper tackles the FBS deployment optimization with imperfect channel estimation and MMSE combining and serves as a starting point in the investigation of pilot assignment techniques for CF-UAV networks. Specifically:

1) A complete and tractable framework is provided to analyze CF-UAV networks, including imperfect CSI, MMSE combining, pilot contamination, and realistic antenna radiation patterns at the UAVs.
2) Closed-form expressions are derived for the local-average signal-to-interference-plus-noise ratio (SINR) when the number of users is large, considering centralized MMSE combining and MMSE channel estimation.
3) Two algorithms are provided for the optimization of the max-min local-average SINR.

This work was supported in part by NSF Award CCF-1815339, by ERC grant 694974, and by the ICREA Academia program.

[1]C. Diaz-Vilor and H. Jafarkhani are with the Center for Pervasive Communications and Computing, Univ. of California, Irvine {cdiazvil, hamidj} at uci.edu

[2]A. Lozano is with Universitat Pompeu Fabra (UPF), Barcelona {angel.lozano} at upf.edu

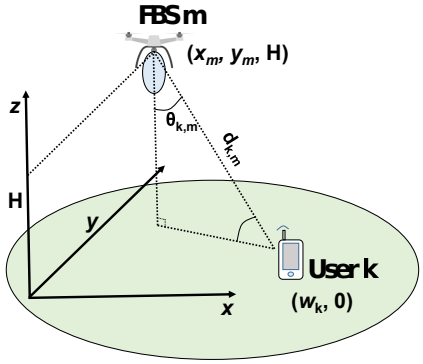

Fig. 1: Geometry for a given transmitter-receiver pair.

II. Network and Channel Model

The CF networks under consideration feature M FBSs with the mth one located at $\boldsymbol{q}_m = (x_m, y_m)$ and altitude H. There are K cochannel single-antenna ground users (GUs) at $\mathbf{w}_k = (\mathrm{x}_k, \mathrm{y}_k)$ for $k = 1, \ldots, K$.

We denote by $g_{k,m}$ the channel coefficient between the kth GU and the mth FBS, following a Rician distribution comprised of (*i*) a dominant LoS component and (*ii*) a Rayleigh-distributed small-scale component. Therefore:

$$g_{k,m} = \sqrt{\frac{\beta_0 g_m(\theta_{k,m})}{d_{k,m}^{\kappa}(K_{k,m}+1)}}\left(\sqrt{K_{k,m}}e^{j\psi_{k,m}} + a_{k,m}\right), \quad (1)$$

where β_0 and κ are the pathloss intercept at a 1-m reference distance and the pathloss exponent, respectively, and $d_{k,m}$ denotes the distance from the kth GU to the mth FBS. The Rician factor is $K_{k,m} = A_1 e^{A_2 \arcsin(\frac{H}{d_{k,m}})}$ for environment-dependent parameters A_1 and A_2 [20]. In addition, $\psi_{k,m} \sim \mathcal{U}[0, 2\pi]$, uniform between 0 and 2π, and $a_{k,m} \sim \mathcal{N}_{\mathbb{C}}(0, 1)$, zero-mean and unit-variance complex Gaussian, respectively, for the phase rotation of the LoS component and for the small-scale fading. Finally, $g_m(\theta_{k,m})$ models the antenna gain at the

mth FBS given the angle $\theta_{k,m}$, as shown in Fig. 1. Based on the analysis provided in [19], [21],

$$g_m(\theta_{k,m}) = 2\,(\alpha_m + 1)\,\cos^{\alpha_m}(\theta_{k,m}), \tag{2}$$

where parameter α_m controls the trade-off between gain and beamwidth. Thus, the overall channel, $g_{k,m}$ is a zero-mean r.v. with average power satisfying

$$r_{k,m} = \mathrm{E}\{|g_{k,m}|^2\} = 2\,(\alpha_m + 1)\,\beta_0\,\frac{H^{\alpha_m}}{d_{k,m}^{\alpha_m+\kappa}}. \tag{3}$$

A. Channel Estimation

Channel estimation is tackled explicitly by means of τ orthogonal pilot sequences of length τ. Let $\boldsymbol{\varphi}_k \in \mathbb{C}^{\tau\times 1}$ be the pilot sequence assigned to the kth user, where $\|\boldsymbol{\varphi}_k\|^2 = \tau$. Upon pilot transmissions by all GUs, the observation at the mth FBS is

$$\boldsymbol{z}_m = \sum_{k=1}^{K} g_{k,m}\,\boldsymbol{\varphi}_k\sqrt{p_k^{\mathrm{t}}} \;+\; \boldsymbol{n}_m, \tag{4}$$

where p_k^{t} is the pilot power of GU k and $\boldsymbol{n}_m \sim \mathcal{N}_{\mathbb{C}}(0, \sigma^2\boldsymbol{I})$. The number of orthogonal pilots is necessarily limited, i.e. $\tau < K$, which gives rise to pilot contamination. Let us denote by $\mathcal{S}_k$ the set of GUs sharing the same pilot sequence with GU k, including GU k. From $\boldsymbol{z}_m$, the mth FBS produces the MMSE channel estimate [22]

$$\hat{g}_{k,m} = \frac{\sqrt{p_k^{\mathrm{t}}\tau}\cdot r_{k,m}}{\sum\limits_{i\in\mathcal{S}_k} p_i^{\mathrm{t}}\tau\cdot r_{i,m} + \sigma^2}\cdot\frac{1}{\sqrt{\tau}}\boldsymbol{\varphi}_k^*\boldsymbol{z}_m. \tag{5}$$

Therefore, the average channel estimate power is

$$\gamma_{k,m} = \mathrm{E}\{|\hat{g}_{k,m}|^2\} = \frac{p_k^{\mathrm{t}}\tau r_{k,m}^2}{\sum\limits_{i\in\mathcal{S}_k} p_i^{\mathrm{t}}\tau\cdot r_{i,m} + \sigma^2}. \tag{6}$$

The channel estimation error, $\tilde{g}_{k,m} = g_{k,m} - \hat{g}_{k,m}$, is uncorrelated with $\hat{g}_{k,m}$ and satisfies $c_{k,m} = \mathrm{E}\{|\tilde{g}_{k,m}|^2\} = r_{k,m} - \gamma_{k,m}$.

B. Uplink Data Transmission

In a given uplink time-frequency resource, the channel matrix is

$$\boldsymbol{G} = \left(\boldsymbol{g}_1, \ldots, \boldsymbol{g}_K\right), \tag{7}$$

where $\boldsymbol{g}_k \in \mathbb{C}^{M\times 1}$ is the channel vector from GU k to all FBSs. Considering (5), the channel matrix can be decomposed as $\boldsymbol{G} = \hat{\boldsymbol{G}} + \tilde{\boldsymbol{G}}$, where $\hat{\boldsymbol{G}}$ is the channel estimate matrix and $\tilde{\boldsymbol{G}}$ is the channel error matrix. To take into account that not every FBS participates in the reception of every GU, we introduce a binary matrix $\boldsymbol{M}^{\mathrm{s}} = (\boldsymbol{m}_1^{\mathrm{s}}, \ldots, \boldsymbol{m}_K^{\mathrm{s}}) \in \mathbb{Z}_2^{M\times K}$ defined as

$$[\boldsymbol{M}^{\mathrm{s}}]_{m,k} = \begin{cases} 1 & \text{if FBS } m \text{ regards GU } k \text{ as signal} \\ 0 & \text{otherwise} \end{cases}. \tag{8}$$

We also define the complementary matrix $\boldsymbol{M}^{\mathrm{i}} = \boldsymbol{1} - \boldsymbol{M}^{\mathrm{s}}$, whose nonzero entries indicate the GUs that each FBS disregards and that therefore constitute interference. In a fully cooperative network, all entries of $\boldsymbol{M}^{\mathrm{s}}$ are equal to one.

At the centralized processing point, the observations from the M APs can be pooled into the vector

$$\boldsymbol{y} = \boldsymbol{M}^{\mathrm{s}}\circ\boldsymbol{G}\boldsymbol{x} + \boldsymbol{M}^{\mathrm{i}}\circ\boldsymbol{G}\boldsymbol{x} + \boldsymbol{n} \tag{9}$$

$$= \underbrace{\boldsymbol{M}^{\mathrm{s}}\circ\hat{\boldsymbol{G}}\boldsymbol{x}}_{\text{signal}} + \underbrace{(\boldsymbol{M}^{\mathrm{s}}\circ\tilde{\boldsymbol{G}} + \boldsymbol{M}^{\mathrm{i}}\circ\boldsymbol{G})\boldsymbol{x} + \boldsymbol{n}}_{\text{noise + interference: } \boldsymbol{v}}, \tag{10}$$

where $\boldsymbol{x} = (\sqrt{p_1}s_1, \ldots, \sqrt{p}_K s_K)^{\mathrm{T}}$, with symbols s_k having unit power, while p_k is the transmit power of GU k, $\circ$ denotes Hadamard product, and $\boldsymbol{n} \sim \mathcal{N}_{\mathbb{C}}(0, \sigma^2\mathbf{I})$. The noise-plus-interference term satisfies $\boldsymbol{\Sigma} = \mathrm{E}\{\boldsymbol{v}\boldsymbol{v}^*\} = \boldsymbol{D}_1 + \boldsymbol{D}_2 + \sigma^2\boldsymbol{I}$, where

$$\boldsymbol{D}_1 = \mathbb{E}\Big\{\big(\boldsymbol{M}^{\mathrm{s}}\circ\tilde{\boldsymbol{G}}\boldsymbol{x}\big)\big(\boldsymbol{M}^{\mathrm{s}}\circ\tilde{\boldsymbol{G}}\boldsymbol{x}\big)^*\Big\} = \mathrm{diag}\left\{\sum_{k\in\mathcal{U}_1} c_{k,1}p_k, \ldots, \sum_{k\in\mathcal{U}_1} c_{k,M}p_k\right\}, \tag{11}$$

and

$$\boldsymbol{D}_2 = \mathbb{E}\Big\{\big(\boldsymbol{M}^{\mathrm{i}}\circ\boldsymbol{G}\boldsymbol{x}\big)\big(\boldsymbol{M}^{\mathrm{i}}\circ\boldsymbol{G}\boldsymbol{x}\big)^*\Big\} = \mathrm{diag}\left\{\sum_{k\notin\mathcal{U}_1} r_{k,1}p_k, \ldots, \sum_{k\notin\mathcal{U}_M} r_{k,M}p_k\right\}, \tag{12}$$

with $\mathcal{U}_m = \{k \,:\, [\boldsymbol{M}^{\mathrm{s}}]_{m,k} = 1\,,\; k = 1, \ldots, K\}$ the set of GUs regarded as signal by the mth FBS.

III. Centralized CF Network with MMSE Subset Reception

Let $\mathcal{F}_k = \{m : [\boldsymbol{M}^{\mathrm{s}}]_{m,k} = 1\;,\; m = 1, \ldots, M\}$ be the subset of FBSs involved in the reception of GU k. From the rows of $\boldsymbol{y}$ whose indices are in $\mathcal{F}_k$, we obtain the $|\mathcal{F}_k|\times 1$ vector

$$\boldsymbol{y}_k = \boldsymbol{M}_k^s\circ\hat{\boldsymbol{G}}_k\boldsymbol{x} + \boldsymbol{v}_k, \tag{13}$$

where

$$\boldsymbol{M}_k^{\mathrm{s}} = (\boldsymbol{m}_{k,1}^{\mathrm{s}}, \ldots, \boldsymbol{m}_{k,K}^{\mathrm{s}}) \in \mathbb{Z}_2^{|\mathcal{F}_k|\times K}, \tag{14}$$

while $\hat{\boldsymbol{G}}_k \in \mathbb{C}^{|\mathcal{F}_k|\times K}$ and $\boldsymbol{v}_k \in \mathbb{C}^{|\mathcal{F}_k|\times 1}$. The MMSE combiner associated with GU k, $\boldsymbol{w}_k \in \mathbb{C}^{|\mathcal{F}_k|\times 1}$, is [7]

$$\boldsymbol{w}_k = \Big(\big(\boldsymbol{M}_k^{\mathrm{s}}\circ\hat{\boldsymbol{G}}_k\big)\boldsymbol{P}\big(\boldsymbol{M}_k^{\mathrm{s}}\circ\hat{\boldsymbol{G}}_k\big)^* + \boldsymbol{\Sigma}_k\Big)^{-1}\hat{\boldsymbol{g}}_k p_k, \tag{15}$$

where $\boldsymbol{P} = \mathrm{diag}(p_1, \ldots, p_K)$. In turn, $\hat{\boldsymbol{g}}_k$ contains the $\mathcal{F}_k$ rows of the M-dimensional channel estimate of GU k, and $\boldsymbol{\Sigma}_k$ is defined similarly. The SINR achieved by GU k is

$$\mathrm{SINR}_{\mathrm{k}} = \hat{\boldsymbol{g}}_k^*\left(\sum_{i\neq k}(\boldsymbol{m}_{k,i}^{\mathrm{s}}\circ\hat{\boldsymbol{g}}_i)(\boldsymbol{m}_{k,i}^{\mathrm{s}}\circ\hat{\boldsymbol{g}}_i)^* p_i + \boldsymbol{\Sigma}_k\right)^{-1}\hat{\boldsymbol{g}}_k p_k, \tag{16}$$

with an ergodic spectral efficiency of

$$\left(1 - \frac{\tau}{\tau_c}\right)\mathbb{E}\{\log_2(1 + \mathrm{SINR}_{\mathrm{k}})\}, \tag{17}$$

where τ_{c} represents the coherence of the channel in symbols and $\frac{\tau}{\tau_{\mathrm{c}}}$ is hence the pilot overhead.

Proposition 1. *For the MMSE subset combiner,*

$$\lim_{K\to\infty} \mathrm{SINR_k} = \sum_{m\in\mathcal{F}_k} \frac{|\hat{g}_{k,m}|^2}{\sum_{i=1}^{\infty} r_{i,m}\, p_i - \gamma_{k,m}\, p_k + \sigma^2}\, p_k.$$

Proof. The proof, omitted for the sake of brevity, hinges on applying Tchebyshev's theorem to (16). □

The expectation of the SINR over the small-scale fading yields the local-average SINR

$$\lim_{K\to\infty} \mathbb{E}\{\mathrm{SINR_k}\} = \sum_{m\in\mathcal{F}_k} \frac{\gamma_{k,m}}{\sum_{i=1}^{\infty} r_{i,m}\, p_i - \gamma_{k,m}\, p_k + \sigma^2}\, p_k. \tag{18}$$

Proposition 2. *For MMSE subset combining with $K \to \infty$, $\mathbb{E}\{\mathrm{SINR_k}\}$ is a decreasing function of $|\mathcal{S}_k|$.*

Proof. Straightforward calculations show that $\mathbb{E}\{\mathrm{SINR_k}\}$ is an increasing function of $\gamma_{k,m}$ and, from (6), $\gamma_{k,m}$ is a decreasing function of $|\mathcal{S}_k|$. □

IV. Problem Formulation

The main motivation of this work is to study the FBS deployment in CF-UAV networks with $\mathbb{E}\{\mathrm{SINR_k}\}$ as the metric to optimize. Defining the set of FBS locations by $\boldsymbol{\mathcal{Q}} = \{\boldsymbol{q}_m \,\text{for}\, m = 1,\dots,M\}$, we can formulate the maximization of the minimum local-average SINR as

$$\max_{\boldsymbol{\mathcal{Q}}} \quad \min_{k} \ \mathbb{E}\{\mathrm{SINR_k}\}, \tag{19}$$

which is nonconvex. Capitalizing on Prop. 1, we study this problem in the regime of large but finite K. To deal with (19), different methods can be utilized to obtain solutions. First, given (18), the gradient can be obtained. By virtue of that, a gradient based (GB) algorithm can be implemented to iteratively update the FBS locations. However, the nonconvexity of the problem may cause the GB method to meet the convergence criteria at early stages, resulting in low quality solutions. To circumvent this challenge, we combine it with the simulated annealing (SA) technique [23], as discussed next.

Given (18) and a large K, then, the optimization problem boils down to

$$\max_{\boldsymbol{\mathcal{Q}}} \quad \min_{k} \ \sum_{m\in\mathcal{F}_k} \frac{\gamma_{k,m}}{\sum_{i=1}^{K} r_{i,m}\, p_i - \gamma_{k,m}\, p_k + \sigma^2}\, p_k, \tag{20}$$

where the optimization variables are subsumed within $\gamma_{k,m}$ and $r_{i,m}$, with $\gamma_{k,m}$ dependant on how pilot sequences are assigned. Hence, the deployment is influenced by: geometric parameters, pilot sequence assignment, and power allocation (on both pilots and data).

From (20), the gradient w.r.t the FBS locations can be derived. For ease of exposition, we proceed with the computation of the derivative w.r.t the horizontal coordinate of the mth FBS,

$$\frac{\partial\, \mathbb{E}\{\mathrm{SINR_k}\}}{\partial x_m} = \frac{\gamma'_{k,m}\left(\sum\limits_{i=1}^{K} r_{i,m}\, p_i + \sigma^2\right) - \gamma_{k,m}\left(\sum\limits_{i=1}^{K} r'_{i,m}\, p_i\right)}{\left(\sum\limits_{i=1}^{K} r_{i,m}\, p_i - \gamma_{k,m}\, p_k + \sigma^2\right)^2}\, p_k, \tag{21}$$

where

$$\begin{aligned}\gamma'_{k,m} &= \frac{\partial \gamma_{k,m}}{\partial x_m} \\ &= \frac{\partial \gamma_{k,m}}{\partial r_{k,m}} \frac{\partial r_{k,m}}{\partial d_{k,m}} \frac{\partial d_{k,m}}{\partial x_m} + \sum_{\substack{i\in\mathcal{S}_k \\ i\neq k}} \frac{\partial \gamma_{k,m}}{\partial r_{i,m}} \frac{\partial r_{i,m}}{\partial d_{i,m}} \frac{\partial d_{i,m}}{\partial x_m},\end{aligned} \tag{22}$$

with

$$\frac{\partial \gamma_{k,m}}{\partial r_{k,m}} = \frac{p_k^{\mathrm{t}} \tau r_{k,m} \left(2\sum_{i\in\mathcal{S}_k} p_i^{\mathrm{t}} \tau r_{i,m} + 2\sigma^2 - p_k^{\mathrm{t}} \tau r_{k,m}\right)}{\left(\sum_{i\in\mathcal{S}_k} p_i^{\mathrm{t}} \tau r_{i,m} + \sigma^2\right)^2}, \tag{23}$$

$$\frac{\partial \gamma_{k,m}}{\partial r_{i,m}} = -\frac{p_i^{\mathrm{t}} p_k^{\mathrm{t}} \tau^2 r_{k,m}^2}{\left(\sum_{i\in\mathcal{S}_k} p_i^{t} \tau r_{i,m} + \sigma^2\right)^2} \qquad i \neq k, \tag{24}$$

and

$$\begin{aligned} r'_{k,m} &= \frac{\partial r_{k,m}}{\partial d_{k,m}} \frac{\partial d_{k,m}}{\partial x_m} \\ &= -\frac{2\,(\alpha_m+1)\beta_0 H^{\alpha_m}}{d_{k,m}^{\alpha_m+\kappa+1}} \cdot \frac{\partial d_{k,m}}{\partial x_m}, \end{aligned} \tag{25}$$

where

$$\frac{\partial d_{k,m}}{x_m} = \frac{x_m - \mathrm{x}_k}{d_{k,m}}. \tag{26}$$

Plugging (23), (24), and (25) into (22), we obtain $\gamma'_{k,m}$, which, in conjunction with (25), yields the derivative w.r.t. x_m. Similarly, formulating the derivative w.r.t. y_m, the overall gradient is obtained with complexity $\mathcal{O}(K + |\mathcal{S}_k|)$. Finally, the GB updates for the max-min $\mathbb{E}\{\mathrm{SINR}_k\}$ problem are

$$\boldsymbol{q}_m^{(j)} \leftarrow \boldsymbol{q}_m^{(j)} + \rho^{(j)} \nabla \mathbb{E}\{\mathrm{SINR_k^{(j)}}\}|_{\boldsymbol{q}_m = \boldsymbol{q}_m^{(j)}}, \tag{27}$$

where j is the GB iteration number and $\rho^{(j)}$ is a decreasing function of j. Due to the nonconvexity of the problem, the updates provided by (27) may quickly converge to local solutions. Therefore, we combine it with the SA, which aims to relocate the FBSs with the objective of further improving $\min \mathbb{E}\{\mathrm{SINR}_k\}$. The core of the SA stage relies on low-SINR users being given a higher weight and the FBS locations being updated accordingly. We use a logarithmic scale, i.e., $L_k = \log_2(C + \mathbb{E}\{\mathrm{SINR}_k\})$, where C is a positive constant ($C = 1$ in our simulations). The main steps are

1) Create the weight vector $\boldsymbol{a} \in \mathbb{R}^{K\times 1}$ in which, with the aim of increasing fairness, users with smaller SINRs are given a higher weight. A possible formulation for $\boldsymbol{a}$ is

$$a_k = \frac{\sum_{i=1}^{K} L_i}{L_k} \left[\max_p \left(\frac{\sum_{s=1}^{K} L_s}{L_p}\right)\right]^{-1} \quad k = 1,\dots,K.$$

2) Displace the FBSs in the direction of the GUs with lower SINRs.

$$\boldsymbol{q}_{m,\mathrm{new}}^{(j)} = \boldsymbol{q}_m^{(j)} + \sum_{k\in\mathcal{U}_m} a_k\, \Psi^{(j)}(\mathbf{w}_k - \boldsymbol{q}_m), \tag{28}$$

where $\Psi^{(j)}$, defined in the next section, is a decreasing function of j for convergence reasons. Note that FBSs

TABLE I: Simulation Parameters

Description	Parameter	Value
GU data power	p_k	100 mW
GU pilot power	p_k^t	100 mW
Path loss reference	β_0	-30 dB
Path loss exponent	κ	2
Dense urban parameters	A_1, A_2	0 , 6.4 dB
FBS altitude	H	20 m
Noise power	σ^2	-120 dBm
Antenna beamwidth	α_m	4
Channel coherence (symbols)	τ_c	1000

only move towards users they are providing service to, i.e., users within $\mathcal{U}_m$.

3) If the update in (27) improves the cost function, the solution is accepted. Else, we compute (28) and accept it if the cost function increases. Otherwise, (28) is accepted with probability $\exp\left(\frac{\mu_{\text{new}}-\mu_{\text{old}}}{T^{(j)}}\right)$, where μ_{old} and μ_{new} are the minimum GU L_k before and after applying (28), respectively. Otherwise, a new neighboring solution is generated from $\boldsymbol{q}_{m,\text{new}}^{(j)} \sim \mathcal{N}(\boldsymbol{q}_m^{(j)}, \Psi^{(j)}\boldsymbol{I})$. Additionally, we define $T^{(j)}$ as the temperature at Iteration j as indicated in the SA literature [23].

Remark. *For small K, the gradient becomes analytically intractable. However, one can still apply the GB updates and the SA, with $\mathbb{E}\{\text{SINR}_k\}$ replaced by its sample mean.*

V. Numerical Results

For the purpose of performance evaluation, we consider a 300m $\times$ 300m wrapped-around universe to avoid boundary effects. Table I lists the parameters used in the simulations, which are based on the CF and UAV literature [5], [14], [15]. Pilot sequences are randomly assigned, with an average reuse factor of K/τ [24]. Unless otherwise specified, $\tau = 70$, with a 7% pilot overhead. As far as $\boldsymbol{M}^{\text{s}}$ is concerned, the $[m,k]$ entry is 1 if $d_{k,m} \leq R_{max}$ for $R_{max} = 50$m. The learning rate of the GB algorithm is $\rho^{(j)} = 200 \cdot 1.005^{-j}$ while, for the SA algorithm, $T^{(j+1)} = 100 \cdot 0.7^j$ and $\Psi^{(j+1)} = 0.0015\frac{\log(4+j)}{\log(2+j)}$. (Changes in the learning rate or in the SA parameters would only affect the speed of convergence.) Finally, the maximum number of iterations for the algorithm is set to 1000.

Simulations are conducted for two different user position distributions, namely square regular grid and Gaussian mixture, denoted by RG and GM in our simulations, respectively. In the latter, user positions are sampled from the mixture

$$f(x,y) = \frac{1}{4}\mathcal{N}(\boldsymbol{m}_1, 35^2\boldsymbol{I}) + \frac{3}{4}\mathcal{N}(\boldsymbol{m}_2, 50^2\boldsymbol{I}),$$

with $\boldsymbol{m}_1 = [55\ 45]$ and $\boldsymbol{m}_2 = [150\ 200]$. Taking as benchmark a square regular grid FBS deployment, we define

$$\text{Gain} = \left(1 - \frac{\tau}{\tau_c}\right) \cdot \frac{\min_k \text{SE}_k^{\text{opt}}}{\min_k \text{SE}_k^{\text{grid}}}, \tag{29}$$

where SE_k^{opt} and $\text{SE}_k^{\text{grid}}$ are the kth user spectral efficiencies after deployment optimization and when the FBSs are arranged in a square regular grid, respectively. Although the optimization is SINR-based, the benefits are quantified in terms of spectral efficiency. We measure the gain over 100 realizations and the results are presented using boxes containing the median, 25th and 75th percentiles, and the most extreme points.

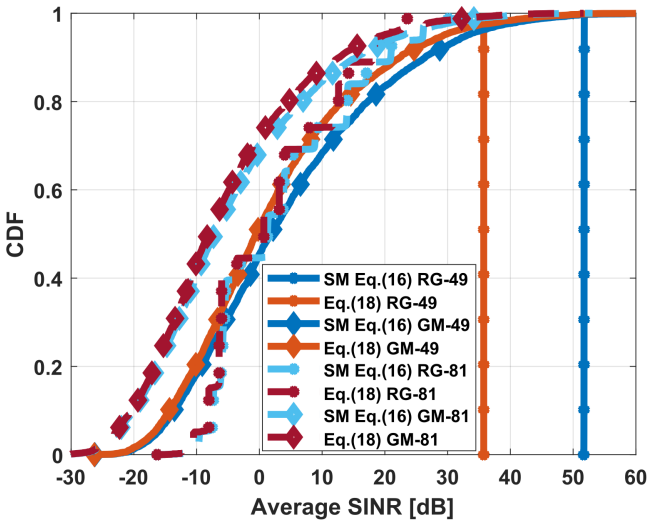

Fig. 2: Local-average SINR using (16) and (18).

We first measure the accuracy of (18) compared to the sample mean (SM) of (16) with the aim of setting a proper value for our large-K simulations. Fig. 2 compares the aforementioned expressions for $M = 49$ under both user distributions for $K = 49$ and $K = 81$. This observation verifies that $K = 81$ makes (18) sufficiently accurate when $M = 49$. Therefore, unless specified, we set $M = 49$ and $K = 81$ in our large-K results.

As mentioned, the performance is influenced by geometry-based parameters, pilot sequence assignment, and power allocation. As the latter is kept homogeneous for all GUs, we focus on the other two. Especially, to understand the impact of pilot contamination and the importance of the FBS optimization even if users conform a square regular grid, we include Figs. 3a and 3b. To create meaningful surface representations, and only for this case, we use $M = 400$ and $K = 625$, which gives a similar M/K per time-frequency resource as the one used throughout this work. Fig. 3a presents $\mathbb{E}\{\text{SINR}\}$ for each GU when there is no pilot contamination, i.e., for $\tau \geq K$. Given the symmetry of the problem, such a deployment is optimal. However, the case of practical interest includes pilot contamination, i.e., $\tau = 300 < K$, whose $\mathbb{E}\{\text{SINR}\}$ is presented in Fig. 3b. The values are lower compared to Fig. 3a and the symmetry is broken, such that a reallocation of the UAVs is able to increase min $\mathbb{E}\{\text{SINR}\}$. Hence, even for homogeneous user distributions, there is a deployment gain because of pilot contamination. There is a further gain associated with geometry-based parameters, such as the GU-FBS distances or how $\boldsymbol{M}^{\text{s}}$ is generated. To quantify these gains, we subsequently provide extensive results.

Figs. 4a and 4b depict the gain for different values of τ for RG and GM user distributions, respectively. We also

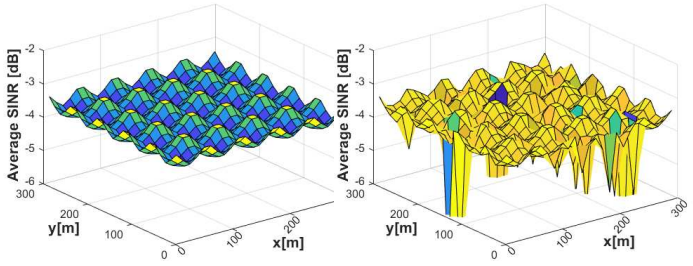

(a) (b)

Fig. 3: $\mathbb{E}\{\text{SINR}\}$ when the user distribution is RG (a) without pilot contamination and (b) with pilot contamination.

include the evolution of the minimum local-average spectral efficiency before and after optimization, denoted by SE^{grid} and SE^{opt}, respectively. Finally, to focus on the gain induced by pilot contamination, we measure it over the same GU locations only varying the pilot assignment between realizations. Clearly, the gain decreases as more pilots are available, i.e., larger τ. This is mainly a consequence of Prop. 2: while having more pilots results in better local-average SINR, and thus higher spectral efficiency, it is more challenging to improve them via optimization. In fact, for the limiting case, i.e., $\tau = K$, the gains in Figs. 4a and 4b originate only from the geometry of the scenario. While for RG there is an average gain at 35% associated to the geometry, for the GM case it increases by a factor of 2.5 given the irregular user distribution, and with the additional pilot gain it achieves a maximum of 710%.

In Figs. 5a and 5b, we include the variation of the gain over M, for a fixed $\tau = 70$ and $K = 81$. For both user distributions, the following conclusion can be extracted: while increasing M results in higher spectral efficiency, the gain tends to decrease, as it is more challenging to improve the FBS deployment. In the limiting case, $M = K$, the gain in the RG case would be one given the symmetry of the problem. However, as depicted in Fig. 5b, for a non-uniform user distribution, the gain remains around 200% as more UAVs can adapt their deployment to the irregularities in the user distribution.

Finally, in Fig. 6, we include the average gain of our method when applied to smaller networks with $M = 25$, $\tau = 70$ and considering $R_{\max} = 50$m and $R_{\max} = 200$m. As $K < \tau$, there is no pilot contamination and therefore the gains originate from the geometric setup of the problem. It is shown that, the more users, the higher the gains. The gains are more pronounced for the GM case, in line with the large-K figures. Finally, considering a smaller $R_{\max}$ results in higher gains as the spectral efficiency is lower, hence easier to improve upon.

VI. Summary

This paper has investigated the FBS deployment problem in CF networks with a realistic system model. We have formulated a max-min $\mathbb{E}\{\text{SINR}_{\text{k}}\}$ optimization problem, which is

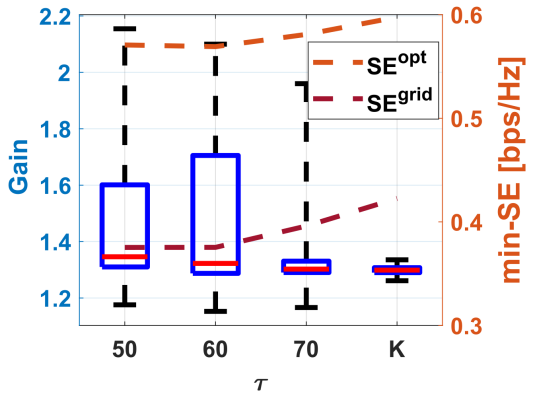

(a)

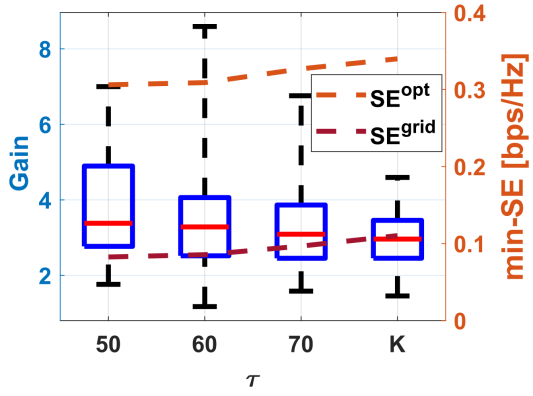

(b)

Fig. 4: Gain vs τ for $K = 81$: (a) RG, (b) GM.

nonconvex and tackled it by means of various algorithms that markedly improve the min-SINR, and therefore the minimum individual spectral efficiency.

References

[1] A. Checko, H. L. Christiansen, Y. Yan, L. Scolari, G. Kardaras, M. S. Berger, and L. Dittmann, "Cloud RAN for mobile networks—A technology overview," *IEEE Commun. Surveys & Tutorials*, vol. 17, no. 1, pp. 405–426, 2014.

[2] S. Venkatesan, A. Lozano, and R. Valenzuela, "Network MIMO: Overcoming intercell interference in indoor wireless systems," in *Asilomar Conf. on Signals, Systems and Computers*, pp. 83–87, 2007.

[3] H. Q. Ngo, A. Ashikhmin, H. Yang, E. G. Larsson, and T. L. Marzetta, "Cell-Free Massive MIMO Versus Small Cells," *IEEE Trans. Wireless Commun.*, vol. 16, pp. 1834–1850, Mar. 2017.

[4] E. Björnson and L. Sanguinetti, "Making Cell-Free Massive MIMO Competitive With MMSE Processing and Centralized Implementation," *IEEE Trans. Wireless Commun.*, vol. 19, pp. 77–90, Jan. 2020.

[5] H. Q. Ngo, L. Tran, T. Q. Duong, M. Matthaiou, and E. G. Larsson, "On the Total Energy Efficiency of Cell-Free Massive MIMO," *IEEE Trans. on Green Commun. and Net.*, vol. 2, pp. 25–39, Nov. 2018.

[6] M. Bashar, K. Cumanan, A. G. Burr, M. Debbah, and H. Q. Ngo, "On the Uplink Max–Min SINR of Cell-Free Massive MIMO Systems," *IEEE Trans. on Wireless Commun.*, vol. 18, pp. 2021–2036, Jan. 2019.

[7] M. Attarifar, A. Abbasfar, and A. Lozano, "Subset MMSE Receivers for Cell-Free Networks," *IEEE Trans. Wireless Commun.*, vol. 19, pp. 4183–4194, Jun. 2020.

[8] G. Interdonato, P. Frenger, and E. G. Larsson, "Scalability Aspects of Cell-Free Massive MIMO," in *2019 IEEE International Conference on Commun. (ICC)*, pp. 1–6, May 2019.

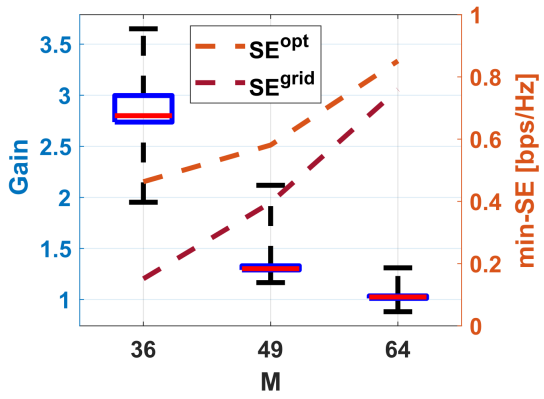

(a)

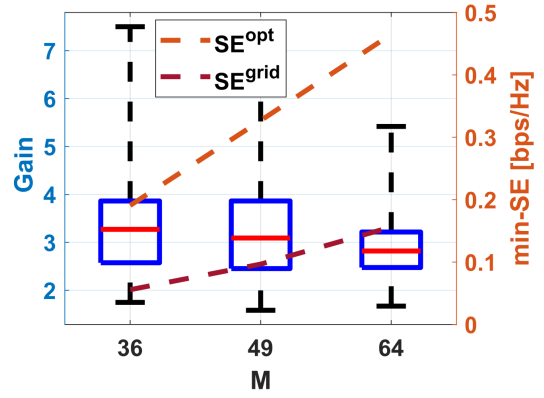

(b)

Fig. 5: Gain vs M for $K = 81$: (a) RG, (b) GM.

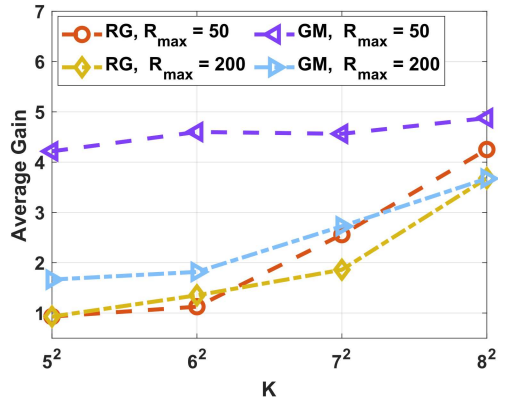

Fig. 6: Gain vs number of GUs in small-K networks.

[9] Y. Zeng, Q. Wu, and R. Zhang, "Accessing From the Sky: A Tutorial on UAV Communications for 5G and Beyond," *Proc. of the IEEE*, vol. 107, pp. 2327–2375, Dec. 2019.

[10] Y. Zeng, J. Xu, and R. Zhang, "Energy Minimization for Wireless Communication with Rotary-Wing UAV," *IEEE Trans. Wireless Commun.*, vol. 18, pp. 2329–2345, Apr. 2019.

[11] Q. Wu, Y. Zeng, and R. Zhang, "Joint Trajectory and Communication Design for Multi-UAV Enabled Wireless Networks," *IEEE Trans. Wireless Commun.*, vol. 17, pp. 2109–2121, Mar. 2018.

[12] F. Cheng, S. Zhang, Z. Li, Y. Chen, N. Zhao, F. R. Yu, and V. C. Leung, "UAV Trajectory Optimization for Data Offloading at the Edge of Multiple Cells," *IEEE Trans. Vehicular Technology*, vol. 67, pp. 6732–6736, Jul. 2018.

[13] C. Shen, T. Chang, J. Gong, Y. Zeng, and R. Zhang, "Multi-UAV Interference Coordination via Joint Trajectory and Power Control," *IEEE Trans. Signal Process.*, vol. 68, pp. 843–858, Jan 2020.

[14] M. Mozaffari, W. Saad, M. Bennis, and M. Debbah, "Unmanned Aerial Vehicle With Underlaid Device-to-Device Communications: Performance and Tradeoffs," *IEEE Trans. Wireless Commun.*, vol. 15, pp. 3949–3963, Jun. 2016.

[15] P. Chandhar, D. Danev, and E. G. Larsson, "Massive MIMO for Communications With Drone Swarms," *IEEE Trans. on Wireless Commun.*, vol. 17, pp. 1604–1629, March 2018.

[16] N. Dao, Q. Pham, N. Tu, T. Thanh, V. Bao, D. Lakew, and S. Cho, "Survey on aerial radio access networks: Toward a comprehensive 6G access infrastructure," *IEEE Commun. Surveys & Tutorials*, vol. 23, no. 2, pp. 1193–1225, 2021.

[17] J. Guo and H. Jafarkhani, "Sensor Deployment With Limited Communication Range in Homogeneous and Heterogeneous Wireless Sensor Networks," *IEEE Trans. on Wireless Commun.*, vol. 15, pp. 6771–6784, Oct. 2016.

[18] E. Koyuncu, M. Shabanighazikelayeh, and H. Seferoglu, "Deployment and Trajectory Optimization of UAVs: A Quantization Theory Approach," *IEEE Trans. on Wireless Commun.*, vol. 17, pp. 8531–8546, Dec. 2018.

[19] J. Guo, P. Walk, and H. Jafarkhani, "Optimal Deployments of UAVs With Directional Antennas for a Power-Efficient Coverage," *IEEE Trans. Commun.*, vol. 68, pp. 5159–5174, Aug. 2020.

[20] S. Shimamoto and Iskandar, "Channel characterization and performance evaluation of mobile communication employing stratospheric platforms," *IEICE Trans. Commun.*, vol. E89-B, pp. 937–944, Mar. 2006.

[21] C. A. Balanis, *Antenna Theory : Analysis and Design*. Wiley, 4th ed., 2016.

[22] S. M. Kay, *Fundamentals of Statistical Signal Processing: Estimation Theory*. Prentice-Hall PTR, 1st ed., 1993.

[23] Peter J. M. van Laarhoven, Emile H. L. Aarts, *Simulated Annealing: Theory and Applications*, vol. 37th. Springer, 1987.

[24] M. Attarifar, A. Abbasfar, and A. Lozano, "Random vs structured pilot assignment in cell-free massive MIMO wireless networks," in *Int'l Conf. Commun. Workshops (ICC Workshops)*, 2018.